Optical properties of monoclinic SnI_2 from relativistic first-principles theory

P. Ravindran, A. Delin, R. Ahuja, and B. Johansson
Condensed Matter Theory Group, Department of Physics, Uppsala University, Box 530, 75121 Uppsala, Sweden

S. Auluck
Department of Physics, University of Roorkee, Roorkee-247 667, India

J. M. Wills
Theoretical Division, Los Alamos National Laboratory, Los Alamos, New Mexico 87545

O. Eriksson
Condensed Matter Theory Group, Department of Physics, Uppsala University, Box 530, 75121 Uppsala, Sweden
and Center for Materials Science and Theoretical Division, Los Alamos National Laboratory, Los Alamos, New Mexico 87545
(Received 12 March 1997)

Within the local-density approximation, using the relativistic full-potential linear muffin-tin orbital method, the electronic structure is calculated for the anisotropic, layered material SnI_2. The direct interband transitions are calculated using the full electric-dipole matrix elements between the Kohn-Sham eigenvalues in the ground state of the system. The inclusion of spin-orbit coupling was found to change the optical properties of this material considerably. Polarized absorption and reflection spectra are calculated and compared with recent experimental results. The experimentally suggested cationic excitation for the lowest-energy transition is confirmed. From the site and angular momentum decomposed electronic structure studies and the detailed analysis of the optical spectra it is found that the lowest-energy transition is taking place between Sn $5s$ (atom type 2a) $\rightarrow$ Sn $5p$ (atom type 4i) states. The ground state calculation was repeated using the tight-binding linear muffin-tin orbital–atomic sphere approximation method, and the resulting band structure agrees very well with the one calculated with the full-potential method. In contrast to recent experimental expectations, our calculations show an indirect band gap, which is in agreement with earlier semiempirical tight-binding calculations as well as with absorption and reflection spectra. [S0163-1829(97)02532-0]

I. INTRODUCTION

The properties of the tin (II) halides have been of interest because of their application in the development of electronic discharge lamps.[1] SnI_2, a layered luminescence semiconductor,[2] has a high color rendering when used in an electric arc lamp.[3] A characteristic feature of this tin di-iodide is its high photosensitivity, which permits its use as a photorecording medium.[4] The spectroscopic properties of SnI_2 such as ionization potentials, dissociation energies, ground state–first excited state energy difference, and first excited state-second excited state energy difference were calculated recently from complete active space self-consistent field calculations.[5] Desai, Rai, and Vyas measured the bulk dielectric constant of SnI_2 as a function of temperature to understand the electric field distribution.[6]

Fujita *et al.*[7,8] have recently studied the polarized absorption and reflection spectra of SnI_2 at a lower temperature and they have found a direct transition at 2.57 eV. The Sn^{2+} ions occupy two inequivalent sites in the monoclinic lattice. Though the experimental results suggest that the cations are responsible for the lowest-energy transition in this material, experimentalists are unable to resolve the exact Sn^{2+} ions responsible for this transition.[9] Hence, theoretical work on the details of the electronic structure and optical properties of this material is required to understand the microscopic origin of the lowest-energy transition.

Gorban *et al.*[2] investigated the photoluminescence, absorption, and reflection spectra of SnI_2 films and found that the forbidden bandwidth for the indirect transition at 86 K is 2.11 eV and that for the direct transition it is 2.59 eV. They also concluded that the conduction band of SnI_2 is formed by the metal ions (i.e., Sn^{2+}). Later, from the detailed study of the fundamental absorption edge based on spectral dependence of the imaginary part of the dielectric constant ϵ_2, Kostyshin *et al.*[4] concluded that the minimum of the conduction band and the maximum of the valence band are located at the same point of the Brillouin zone. Very recently Ohno *et al.*[8] measured the polarized absorption and reflection spectra of SnI_2 in the fundamental absorption region at temperatures 10–300 K. From the spectral dependence of the absorption edge with temperature they concluded that the lowest-energy gap of SnI_2 is of a direct type. Doni *et al.*[10] have obtained the electronic band structure using the overlap reduced semiempirical tight-binding method and shown that SnI_2 has an indirect fundamental gap of about 2.1 eV, followed by a region of weak direct transitions. It is interesting to note that there is a controversy regarding the nature of the band gap in SnI_2 not only between theory and experiment but also between the experimental studies. Thus, more accurate electronic structure studies on SnI_2 are required to confirm the nature of the band gap. This is one of the motivations for the present investigation. Detailed studies of the chemical bonding nature of SnI_2 are also particularly inter-

esting because its closely related system SnI_4 has an unusual behavior of pressure induced amorphization.

Because of the complicated nature of the band structure, Doni *et al.*[10] studied the electronic properties of SnI_2 by introducing a model hexagonal lattice, obtained from slight distortions of the monoclinic lattice. In the present paper we have not made this simplifying assumption. All calculations presented here are thus performed using the correct crystal structure. Though several experimental studies are available regarding optical properties of SnI_2,[2,4,7,8] no theoretical attempt has yet been made to understand the microscopic origin of the experimentally observed optical transitions. Hence, the present study is a detailed investigation on the electronic structure and optical properties of SnI_2 using a state of the art full potential linear muffin-tin orbital (FP-LMTO) method. As a complement to the highly accurate but computationally very heavy full-potential calculations, we also performed tight-binding–LMTO calculations in the atomic sphere approximation (TB-LMTO-ASA). Few explicit comparisons between a very accurate method like the FP-LMTO, and a simpler method, like TB-LMTO-ASA, have been done for systems with very open structures. Therefore, such a comparison is interesting in itself. Moreover, due to the simpler interpretation of the electronic structure it is helpful to perform ASA calculations in parallel to full-potential calculations. For instance, all orbital-projected quantities are better defined in the atomic sphere approximation, where an interstitial regime is absent.

The rest of this paper is organized as follows. The theoretical methods used are described in Sec. II. Section III deals with the crystal structure and chemical bonding nature of SnI_2 using charge-density studies and angular momentum and site decomposed density of states (DOS) analysis. The band structure obtained from FP-LMTO and the site and angular momentum projected band structure obtained from TB-LMTO method are given in Sec. IV. The polarized absorption and reflectivity spectra obtained from the full-potential–LMTO method and other optical properties are given in Sec. V where they are compared with available experimental results. The most important conclusions drawn from our theoretical studies are given in Sec. VI.

II. COMPUTATIONAL DETAILS

A. TB-LMTO method

In the part of our study where the ASA was used, the Hamiltonian and overlap matrices were evaluated over atomic spheres where the potential is spherically symmetric. For solving the one-electron Schrödinger-like equation self-consistently we have used the scalar-relativistic linear muffin-tin orbital method in the ASA, including the combined correction terms.[11] In the ASA the selection of sphere radii is very important, in particular for the open low symmetry structures such as that of SnI_2.[12] In order to achieve that the overlap between the spheres is less than 20%, we have included 23 empty spheres in ten different equivalent positions in the primitive cell of the base-centered monoclinic lattice. With this configuration, if we adopt the procedure given by Jepsen and Andersen[12] for the selection of sphere radii, the calculated overlap between the spheres are within 17%. Among the ten types of empty spheres, two types occupy the 8j position, seven types occupy the 4i position, and the remaining one occupies the 2*c* position of the $C2/m$ lattice. Hence, the calculation involves totally 32 spheres of 15 different types. Although this large number of empty spheres in a calculation might seem deterrent, the particular implementation of the TB-LMTO-ASA used makes the determination of the both symmetry and optimal sphere radii extremely easy. Also, the TB-LMTO-ASA calculations are very fast and the computational effort involved is minute compared to the FP-LMTO calculations.

The basis set consists of tin $5s$, $5p$, iodine $5p$ and empty sphere $1s$ LMTO's. The Sn $5d$ and $4f$, iodine $6s$, $5d$, and $4f$, and the empty sphere p and d partial waves were included in the tails of the above mentioned LMTO's. This treatment corresponds to Löwdin down-folding of the high block (i.e., Sn $5d$, $4f$ and I $6s$, etc.) of the secular matrix followed by energy linearization of the resulting low block (i.e., Sn $5s$, $5p$ and I $5p$, etc.). This treatment not only reduces the size of the secular matrix, but also serves to avoid distortions of the phase shifts of the high partial waves.[11] The basis functions were calculated at fixed energies E_ν, which were chosen to be at the center of gravity of the occupied parts of the site and angular momentum projected bands. The core states are treated relativistically, while the valence states were calculated scalar relativistically, i.e., except for the spin-orbit coupling all the other relativistic effects were incorporated.

The tetrahedron method for the Brillouin zone (i.e., k space) integrations has been used, in its latest version, according to Blöchl *et al.*,[11] which avoids misweighing and corrects errors due to the linear approximation of the bands inside each tetrahedron. The von Barth–Hedin parametrization is used for the exchange correlation potential within the local density approximation. 320 k points were included in the iterations towards self-consistency. The self-consistency iterations were continued until the total energy difference between two consecutive iterations was less than 10^{-6} Ry. Though more complications are involved in those calculations, the band structure obtained from this computationally efficient method was found to be in good agreement with the highly accurate FP-LMTO method. Furthermore, the particular implementation of the TB-LMTO-ASA used here is very convenient for viewing and analyzing the orbital-projected band structures, which proved to be very useful in the subsequent analysis of the electronic structure of SnI_2.

B. FP-LMTO method

The full-potential–LMTO calculations[13] were all electron, fully relativistic with the spin-orbit coupling included at each variational step. Furthermore, no shape approximation to the charge density or potential was used. The base geometry consists of a muffin-tin part and an interstitial part. Inside the muffin-tin part the basis functions, charge density, and potential were expanded in symmetry adapted spherical-harmonic functions together with a radial function and in a Fourier series in the interstitial. The spherical-harmonic expansion of the charge density, potential, and basis functions were carried out up to $\ell_{\max}=6$. The basis set was comprised of augmented linear muffin-tin orbitals.[11] The tails of the basis functions outside their parent spheres were linear com-

TABLE I. The structural parameters used in the present calculations. Three different sets of x and y atomic position parameters are given for iodine in the 4(i) position. To distinguish these atoms the atom positions for iodine in different equivalent positions are represented by 4(ia), 4(ib), and 4(ic). The lattice parameters are in Å.

System SnI_2	$Z=6$	Space group $C2/m$ (No. 12)	Pearson symbol $mC18$	
Lattice parameters	$a=14.17$	$b=4.535$	$c=10.87$	$\beta=92.0°$
Atom	Position	x	y	z
Sn(1)	2(a)	0.0000	0.0000	0.0000
Sn(2)	4(i)	0.2662	0.0000	0.3065
I(1)	4(ia)	0.0780	0.0000	0.7299
I(2)	4(ib)	0.3602	0.0000	0.5609
I(3)	4(ic)	0.3523	0.0000	0.9239

binations of Hankel or Neuman functions depending on the sign of the kinetic energy κ^2 (the kinetic energy of the basis function in the interstitial region). The basis included $5s$, $5p$, $5d$, and $4f$ partial waves of both tin and iodine. In an attempt to give a better description of the optical properties, the pseudocore Sn $4d$ and the high lying I $6s$ orbitals were also included. However, their effect on the spectra was found to be minor.

We used two tail energies for every state. The integrations over the Brillouin zone in the ground state calculation were carried out as a weighted sum, using the special point sampling,[14] with weights reflecting the symmetry of a given k point. We also used a Gaussian smearing width of 20 mRyd for each eigenvalue in the vicinity of the Fermi level to speed up the convergence. For the DOS and optical calculations, the tetrahedron integration method was employed. The calculations were done at the experimentally determined structural parameters given in Table I and the volume ratio between the interstitial region and the unit cell was approximately 0.65. The exchange and correlation were treated in the local-density approximation using the von Barth–Hedin exchange correlation functional with parameters given by Janak *et al.*.[15] The results reported here used 512 k points in the full base-centered monoclinic Brillouin zone (BZ). We have tested the k-space convergence of our results by performing the same calculation with 343 k points in the full BZ. Although some peaks changed just as in the tests of the basis size, the overall change in the results was minor. We thus conclude that our calculation is satisfactorily converged.

Since both tin and iodine are heavy elements, it is expected that the spin-orbit interaction should be significant. In order to test this we performed the FP-LMTO calculations both with and without the spin-orbit term, but with the scalar-relativistic terms included in both calculations. When calculating the optical matrix elements, we considered the momentum operator but neglected the spin-flip term.[16]

C. Optical properties

The optical properties of matter can be described by means of the transverse dielectric function $\epsilon(\mathbf{q},\omega)$ where $\mathbf{q}$ is the momentum transfer in the photon-electron interaction and ω is the energy transfer. At lower energies one can set $\mathbf{q}=\mathbf{0}$, and we arrive at the electric-dipole approximation, which is assumed throughout this paper. The real and imaginary parts of $\epsilon(\omega)$ are often referred to as ϵ_1 and ϵ_2, respectively. We have calculated the dielectric function for frequencies well above those of the phonons and therefore we considered only electronic excitations. The dielectric function may be calculated using the random-phase approximation and we neglected local field and finite lifetime effects.[17] In condensed matter systems, there are two contributions to $\epsilon(\omega)$, namely, intraband and interband transitions. The contribution from intraband transitions is important only for metals. The interband transitions can further be split into direct and indirect transitions. The indirect interband transitions involve scattering of phonons and are neglected here. It is expected that the indirect transitions give only a small contribution to $\epsilon(\omega)$ in comparison to the direct transitions,[18] although the indirect transitions will have a broadening effect. How large this effect is depends on the temperature. Also other effects, e.g., excitons, affect the optical properties, specifically, excitons normally give rise to rather sharp peaks.

The direct interband contribution to the imaginary part of the dielectric function, $\epsilon_2(\omega)$ is calculated by summing all possible transitions from the occupied to unoccupied states, taking the appropriate transition matrix element into account. The dielectric function is a tensor and all the components need to be calculated. However, we have chosen our principal axes so that the only nonzero off-diagonal element in ϵ is ϵ^{xz} (and, of course ϵ^{zx}). The amplitude of ϵ^{xz} was seen to be negligible in comparison to the amplitude of the diagonal elements. This is simply due to the fact that the angle between the z and x axes, β, is 92°, so that our principal axes are close to form an orthogonal coordinate system. Therefore we can restrict our considerations to the diagonal matrix elements $\epsilon^{\nu\nu}(\omega)$ with $\nu=x$, y, or z. The interband contribution to the diagonal elements of $\epsilon_2(\omega)$ is given by

$$\epsilon_2^{\nu\nu}=\frac{8\pi^2e^2}{m^2\omega^2}\sum_{n}^{\text{unocc}}\sum_{n'}^{\text{occ}}\int_{\text{BZ}}|P^{\nu}_{nn'}(k)|^2 f_{kn}(1-f_{kn'})\times\delta(E^k_n-E^k_{n'}-\hbar\omega)\times\frac{d^3k}{(2\pi)^3}, \tag{1}$$

where e is the electron charge, m its mass, f_{kn} the Fermi distribution function, and $P^{\nu}_{nn'}$ is the projection of the momentum matrix elements along the ν direction of the electric

field. E_n^k are the one electron energies. The evaluation of matrix elements in Eq. (1) is done over the muffin-tin and interstitial regions separately. Further details about the evaluation of matrix elements are given elsewhere.[19] The integration over the Brillouin zone in Eq. (1) is performed using a linear interpolation on a mesh of uniformly distributed points, i.e., the tetrahedron method. The total $\epsilon_2^{\nu\nu}$ was obtained from $\epsilon_2^{\nu\nu}$(IBZ), i.e., $\epsilon_2^{\nu\nu}$ was calculated only in the irreducible part of the BZ using

$$\epsilon_2 = \frac{1}{N}\sum_{i=1}^{N} \sigma_i^T \epsilon_2(\mathrm{IBZ})\sigma_i , \tag{2}$$

where N is the number of symmetry operations and σ_i represents the symmetry operations. For shortness, the symbol $\epsilon(\omega)$ is used instead of $\epsilon^{\nu\nu}(\omega)$. Lifetime broadening was simulated by convoluting the absorptive part of the dielectric function with a Lorenzian, whose full width at half maximum (Δ_{FW}) is equal to $0.005(\hbar\omega)^2$ eV. The experimental resolution was simulated by broadening the final spectra with a Gaussian of constant Δ_{FW} equal to 0.01 eV.

After having evaluated Eq. (1) we calculated the interband contribution to the real part of the dielectric function $\epsilon_1(\omega)$ from the Kramers-Kronig relation

$$\epsilon_1(\omega) = 1 + \frac{2}{\pi} P \int_0^{\infty} \frac{\epsilon_2(\omega')\omega' d\omega'}{\omega'^2 - \omega^2} . \tag{3}$$

In order to calculate $\epsilon_1(\omega)$ one needs to have a good representation of $\epsilon_2(\omega)$ up to high energies. In the present work we have calculated $\epsilon_2(\omega)$ up to 41 eV above the Fermi level, which also was the truncation energy used in Eq. (3). We tested the convergence of this approach by performing test calculations (with fewer k points and a smaller basis) where the truncation energy was varied. These calculations showed that good convergence was obtained for truncation energies above 40 eV.

To compare our theoretical results with the experimentally observed polarized reflectivity spectra we have calculated those spectra using the following relation. The specular reflectivity can be obtained from the complex dielectric constant given in Eq. (2) through the usual Fresnel's equation,

$$R^{\nu\nu}(\omega) = \left| \frac{\sqrt{\epsilon(\omega)} - 1}{\sqrt{\epsilon(\omega)} + 1} \right|^2 . \tag{4}$$

Note that this formula assumes that the polarization of the incoming light and the measured light is the same. Different polarization directions couple through the off-diagonal elements and we can therefore expect such effects to be minor in the present studies since the term ϵ^{xz} is very small. We also calculated the absorption coefficient $I(\omega)$ and the electron energy-loss spectrum $L(\omega)$ using the following expressions:

$$I(\omega) = 2\omega \left(\frac{[\epsilon_1^2(\omega) + \epsilon_2^2(\omega)]^{1/2} - \epsilon_1(\omega)}{2} \right)^{1/2} , \tag{5}$$

$$L(\omega) = \frac{\epsilon_2(\omega)}{\epsilon_1^2(\omega) + \epsilon_2^2(\omega)} . \tag{6}$$

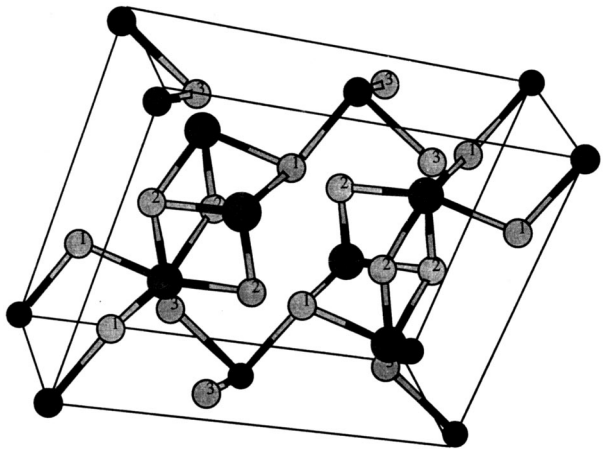

FIG. 1. The crystal structure of SnI_2. The black balls are the Sn atoms, where small black balls refer to Sn(2a) and big black balls represent Sn(4i). The gray balls are the iodine atoms, where 1, 2, and 3 refer to iodine in the 4ia, 4ib, and 4ic positions, respectively. The atom positions are explicitly given in Table I.

III. CRYSTAL STRUCTURE AND CHEMICAL BONDING

A. Crystal structural aspects

Howie *et al.*[21] made the crystal structural analysis of SnI_2. The reported structure is monoclinic with distinct layers having three inequivalent positions for the iodine atoms, which was later confirmed by nuclear quadrupole resonance frequencies measurements.[22] The crystal structure of the layered SnI_2 is shown in Fig. 1. The structural parameters used in the present calculations are given in Table I. In this structure, the most tightly bonded pairs of Sn-I ions are packed in puckered sheets along the (201) plane with weaker bonds linking adjacent layers. Two such puckered sheets exist per unit cell of SnI_2 and are depicted with bonds in Fig. 1. Each unit cell contains six SnI_2 molecules. The Sn^{2+} ions occupy two inequivalent sites. One third of the Sn^{2+} ions [small black balls in Fig. 1, 2(a) position in Table I] are surrounded almost octahedrally by six iodine ions as is the case of Pb^{2+} ions in PbI_2. The remaining Sn^{2+} ions [big black balls in Fig. 1, 4(i) position in Table I] occupy the sites similar to those of the Pb^{2+} ions in the orthorhombic $PbCl_2$ crystal where each cation is surrounded by six halogen ions at the corners of a trigonal prism. The SnI_2 structure may be viewed as a distortion from a simple cubic-like-structure where one Sn atom and two I atoms are stacked in different atomic layers when moving in the 111 direction of the simple cubic Bravais lattice.

B. Chemical bonding

In SnI_2 each Sn(2a) atom is surrounded by two I(4ia) atoms at a distance 5.996 a.u. and four I(4ic) atoms at a distance 6.001 a.u. Further, each Sn(4i) atom is surrounded by one I(4ib) atom at 5.720 a.u., two I(4ia) atoms at 6.045 a.u., and two more I(4ia) atoms at 6.154 a.u. This indicates that the strongest bonding in this solid is between Sn(4i) and I(4ib) and that it has a dominant covalent character. The low value of the bond length between atoms with few nearest neighbors is in line with the observation of Pauling.[23] The larger value of the bond length between Sn(2a) with neigh-

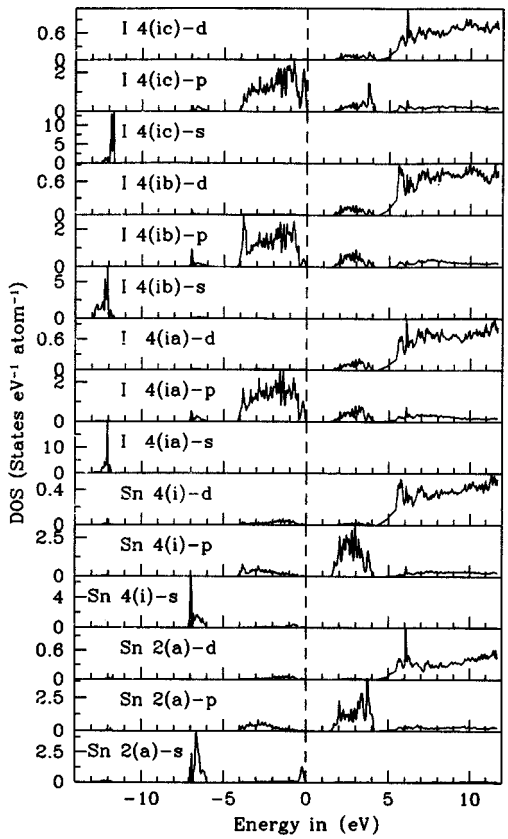

FIG. 2. The angular momentum and site decomposed density of states of SnI_2 from the spin-orbit coupling included full-potential–LMTO method.

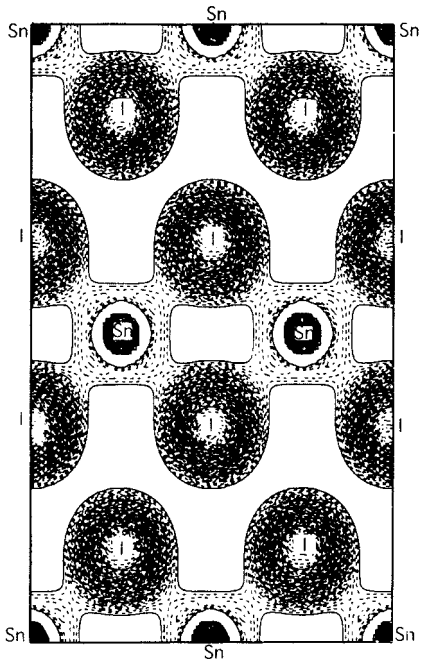

FIG. 3. The valence charge distribution of SnI_2 in the (110) plane. 90 contours are drawn between 0.01 and 0.1 electrons/a.u.^{3}.

boring iodine in comparison with that of Sn(4i) indicates that the nature of the chemical bonding of tin in the two different equivalent sites in this material is somewhat different. Our charge-density distribution analysis as well as DOS analysis, discussed below, shows that the chemical bonding of Sn(2a) with neighboring iodine is more ionic in nature compared with that of Sn(4i). This different nature of bonding behavior significantly changes the electronic structure and optical properties SnI_2 and is discussed in detail in Secs. IV and V.

The angular momentum and site decomposed density of states of SnI_2 are shown in Fig. 2. From this figure it can be seen that the $5p$ population on the tin sites is much lower than that of the ground state atomic configuration. At the same time the electron population in the $5p$ states of iodine is considerably increased compared with the ground state atomic configuration. Thus, there is definitely an ionic character of the bond between Sn and I. This is reasonable, because the difference in Pauling's electronegativity between Sn and I is 0.7, which is considerable. In support of the above viewpoint the Mulliken population analysis of SnX_2 ($X=\mathrm{Cl,Br,I}$) by Benavide-Garcia and Balasubramanian[5] also shows that the tin atom exhibits population deficiency from its neutral atomic population for all cases while the halogen atoms exhibit excess electronic density confirming the ionicity in SnI_2.[5] Further, Fig. 2 shows that in the energy region where the I p have the most weight, -4–0 eV, there are also Sn p and Sn d states. As discussed in previous studies,[24,25] this indicates the existence of covalent bonding between tin and iodine. In addition, the low symmetry of this compound and the directional bonds are clear indications of the covalent nature of the bonding.

Figure 3 presents the contour plots of the total valence charge distribution of SnI_2 in the ab plane. The charge-density contours show that the bonding between the layers is weaker, with a low electron density in this region. The electronic charge densities have enabled us to investigate the bonding in this compound. The main feature is a strong interaction in the puckered Sn-I net. The contour plot shows that most of the electrons are accumulated around the iodine sites in this compound, whereas the population of electrons in the tin sites is smaller. This, of course, is due to the ionic bonding between tin and iodine.

The electronic structure and charge-density distribution hence give evidence for a chemical binding in SnI_2 which is a combination of ionic and covalent bonds. The covalent nature is also consistent with the fact that the structural arrangement may be viewed as a distortion of a simple cubic type of stacking, where, as a consequence of the distortion, Sn-I bonds are strengthened enhancing the covalent character of the binding. As a matter of fact one may approximate the electronic structure of SnI_2 by that of a simplified simple cubic type structure (data not shown).

IV. BAND STRUCTURE

The band structure of SnI_2, including spin orbit coupling (SOC), obtained from the FP-LMTO method is given in Fig. 4. A calculation neglecting the SOC gave rather similar results and is therefore not displayed. The regions below the Fermi level in Fig. 4 contains 27 bands, which can be divided into three regions: the bottommost valence-band region, the middle of the valence-band region, and the top of the valence-band region. The bottommost valence band is

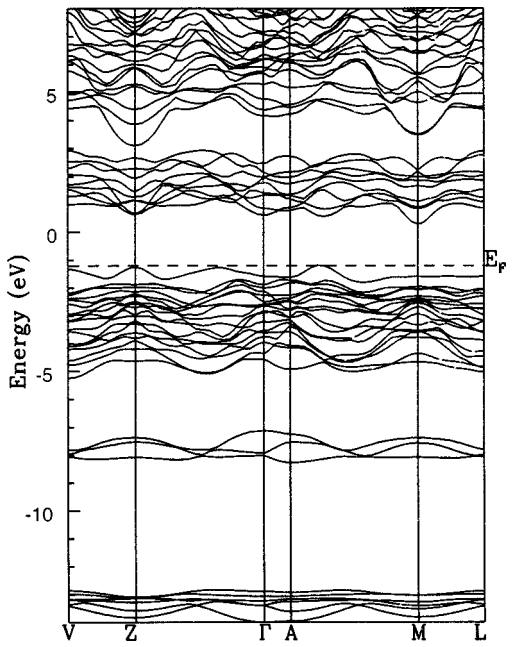

FIG. 4. The band structure of SnI_2 with spin-orbit coupling from full-potential–LMTO method.

around 13 eV below the Fermi level and contains six bands arising from the iodine 5*s* states. The middle of the valence-band region contains three bands, located around 8 eV below the Fermi level. They have mostly cation Sn^+ 5*s* character. Among these three bands, the bottom two are dominated by 5*s* states of Sn in the 4(i) position and the top one is dominated by the 5*s* states of Sn in the 2(a) position. These cation 5*s* states hybridize mostly with the iodine 5*p* states as is clear from Fig. 2. As it turns out, this hybridization is very important for the optical properties of this compound, since much of the interband transitions take place between these cation 5*s* states and the conduction band. In order to acquire a better understanding of the band structure of this layered material, we calculated (using the TB-LMTO-ASA method) the orbital-projected band structure of SnI_2 and this is presented in Figs. 5 (Sn states) and 6 (I states). The width of the orbital-projected bands is proportional to the weight(s) of the corresponding orthonormal orbital(s).[11] The iodine 5*p* bands lie very low in energy and are not shown in Figs. 5 and 6. From Fig. 5 it is clear that the Sn 5*s* bands are located at different energies depending on the spatial position of the cation within the unit cell.

The top of the valence-band region contains 18 bands and among those bands there is one broadband which is closer to the Fermi level and is distinctly separated from the others. The interesting aspects of the band structure of this material is that even though the Sn(2a) 5*s* bands are around 6 eV away from the Fermi level, they contribute significantly to this single band. This is due to the hybridization between Sn(2a) with I(4ia) and I(4ic), which is clearly seen in the orbital-projected bands given in Fig. 5 and the site and angular momentum projected DOS given in Fig. 2. Because of the ionicity, the tin 5*p* electrons are mainly above E_F and hence their contribution to the valence band is smaller.

The conduction-band region consists of nine bands located between 0 and 3 eV, having predominantly Sn 5*p* character. Among the nine bands, the bottommost six bands

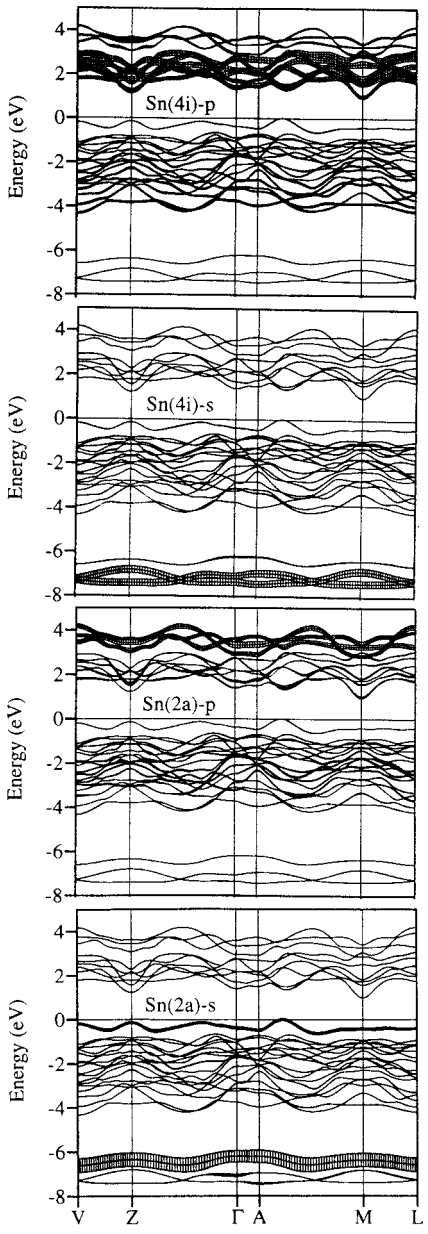

FIG. 5. The orbital-projected band structure of tin in SnI_2 obtained from the scalar-relativistic TB-LMTO method.

arise mostly from the 5*p* states of Sn in the 4i position and the top three bands are mainly from 5*p* states of Sn in the 2a position. Once again these features clearly demonstrate that the bonding behavior of Sn in the two inequivalent sites is different. Above the Sn *p* bands, there is a cluster of bands ~3.5 eV above the Fermi level. The origin of these bands is the 5*d* states of both iodine and tin as is clearly seen from the site and orbital-projected DOS shown in Fig. 2.

As mentioned earlier, there is a contradiction regarding the nature of the band gap in this material, not only between experiment and theory but also between different experimental studies. The present energy-band structure shows that the topmost valence band is studied between the *A* and *M* points and the bottommost conduction band is at the *M* point of the Brillouin zone (Fig. 4). This clearly shows that the nature of the band gap in this material is of an indirect type. This

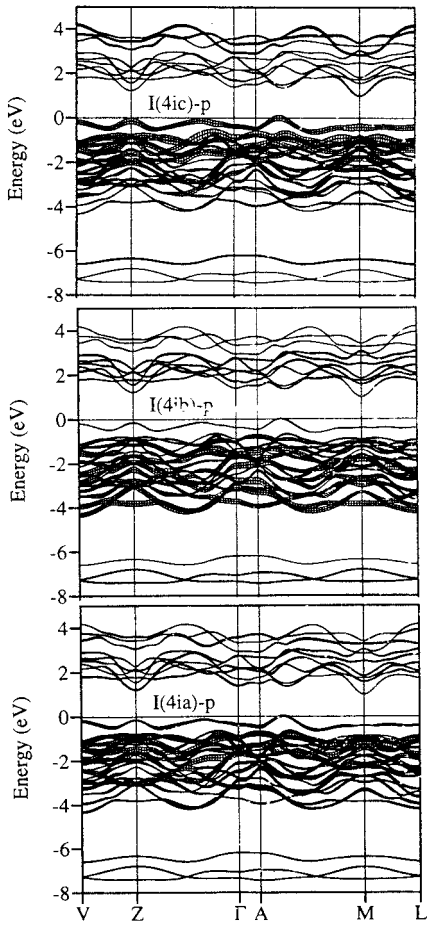

FIG. 6. The orbital projected band structure of iodine in SnI_2 obtained from the scalar-relativistic TB-LMTO method.

observation is consistent with the conclusion arrived at by Doni *et al.*,[10] the absorption as well as reflectivity measurements by Garbon *et al.*,[2] but against the conclusion arrived at by Kostyshin *et al.*[4] from absorption measurements on thin films and Fujita *et al.*[7] from single crystal reflectivity and absorption measurements. Our orbital-projected band-structure studies (obtained by means of TB-LMTO-ASA method) show that the bottom of the conduction band at the M point is mainly of p_x character originating from Sn at the 4i position. Further, we notice that the topmost valence band arises mostly from Sn(2a) s states hybridizing with p_z of I(4ia) and with the p_x, p_y, and p_z of I(4ic). The band gap of SnI_2 without the spin-orbit coupling gives a value of 1.54 eV and with the spin-orbit coupling a value of 1.37 eV. These values are smaller than the experimental measurements by Kostyshin *et al.*[4] (2.52 eV at 85 K), Gorban *et al.*[2] (2.2 eV at 86 K), and Fujita *et al.*[7] (2.275 eV). The calculated band gap is identified here with the difference between the highest occupied and the lowest unoccupied Kohn-Sham eigenvalues, the so-called Kohn-Sham gap. The real band gap, however, is the smallest difference between the energy required to remove an electron from the valence band of the insulating N-particle ground state to infinity and the energy obtained by adding an electron to the conduction band of the insulating N-particle ground state. This real band gap can be written as a sum of the Kohn-Sham gap and a part originating from the discontinuity in the exchange-correlation potential at the integer particle number N.[26] Because of the difficulties with the discontinuity, there are no standard methods for calculating (correctly) the size of band gaps, although recent work based on the GW approximation seems promising in this regard.[27,28] We have not explored this theory here and for the lack of a better theory we empirically increased the band gap until it coincided with the experimentally measured value. In the calculation of the optical spectra we have therefore artificially increased the gap with 0.8 eV. This value was determined by comparing the peak positions in the experimental and theoretical reflectivity spectra measured by Fujita *et al.*[7] Since the agreement between theory and experiment is, as will be clear below, somewhat limited, this value is quite uncertain and might instead of 0.8 eV be as large as 1 eV or more.

As a final remark in this section we note that the electronic structure obtained from the LMTO-ASA and FP-LMTO methods is rather similar. It is interesting that an approximation which is based on spherical averages throughout the crystal works well even for a rather loose-packed structure, provided one takes care in filling open voids in the structure by so-called ''empty spheres.''

V. RESULTS FROM OPTICAL PROPERTIES

Further insight into the electronic structure can be obtained by studying the optical properties. The optical functions reflect the fine structure of the energy distribution of the electron states in the valence and conduction bands. In our investigation of optical properties we have first calculated the imaginary part of the dielectric function directly from Eq. (1). There are eight prominent peaks appearing in the $\epsilon_2(\omega)$ spectra, denoted by A,B,C, etc. in Fig. 7. Now we will try to explain the origin of these peaks based on our electronic structure studies. As discussed in Sec. IV, there are 27 bands in the valence-band region (see Fig. 4). The lowest-energy peak A in Fig. 7 is due to band 27 $\rightarrow$ band 28 interband transition [i.e., mostly Sn(2a) $5s \rightarrow$ Sn(4i) $5p$ with small contribution from I($5p$) $\rightarrow$ I,Sn $5d$]. This peak has also been observed by Kostyshin *et al.*[4] from the experimental near fundamental edge reflectivity and absorption measurements. These authors concluded that this peak structure is due to direct interband transitions, which is consistent with our theoretical observation. When claiming that an interband transition is taking place between two different atoms, as we have done in the notation used above, we do not mean that the final and initial states are in completely different regions of space. The mentioned atoms signify the origin of the states involved, not their positions in space. Peak B in Fig. 7 is caused by transitions from band 27 to bands 28 and 29. The $5s$ and $5p$ electrons of both Sn(2a) and Sn(4i) are involved in the interband transitions responsible for the peaks C, D, and E in Fig. 7. Sn($5d$) $\rightarrow$ Sn($5p$) as well as I($5p$) $\rightarrow$ I ($5d$) interband transition also takes place in this region. The peaks F and G originate from the Sn($5s$) $\rightarrow$ Sn($5p$) as well as I($5p$) $\rightarrow$ Sn,I($5d$) interband transitions. Further, the highest-energy peak in the $\epsilon_2(\omega)$ spectra (i.e., G) is due to the direct interband transition from Sn,I($5p$) $\rightarrow$ Sn,I($5d$). Because of the presence of a cluster of broad Sn($5d$) and I($5d$) bands in the high-energy part of the conduction band

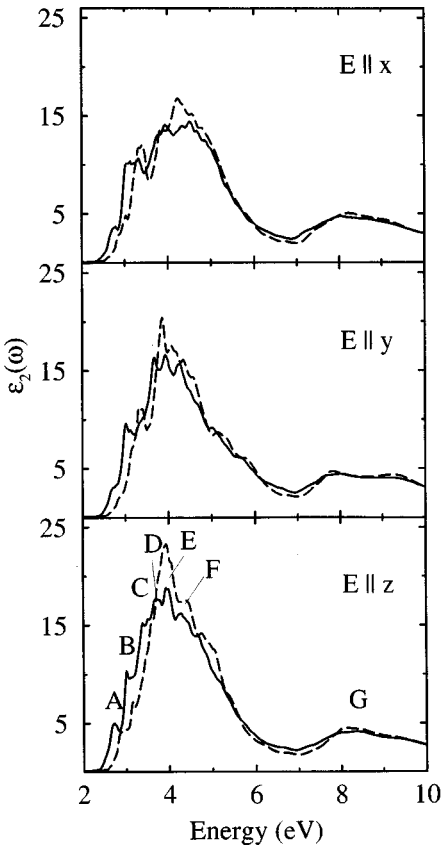

FIG. 7. The imaginary parts of the diagonal elements of the dielectric tensor of SnI_2 with spin-orbit coupling. The spectra are slightly broadened, see text.

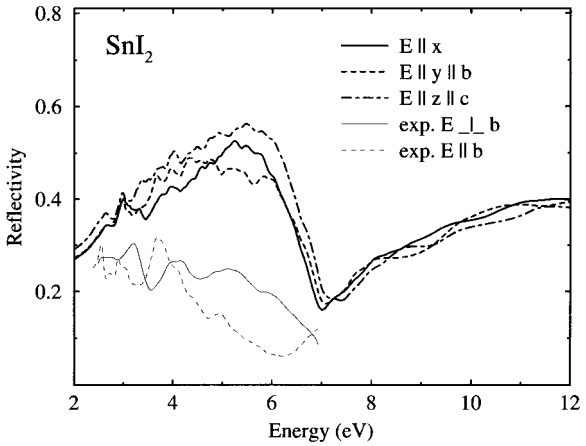

FIG. 8. Calculated and experimental (Ref. 7) reflectivity spectra of SnI_2. The calculated spectra are illustrated with thick lines, whereas the experimental spectra are drawn with thin lines. The solid lines should be compared with each other, and the same is valid for the dashed lines. No experimental measurement corresponding to our calculated dot-dashed spectrum has been performed. The calculated spectra are slightly broadened, see text.

in SnI_2, there is very little structure appearing in the high-energy part of the optical spectra.

Very recently, Fujita *et al.*[7] measured the polarized reflectivity spectra for SnI_2 at low temperatures. In order to compare with the experimental reflectivity spectra, we have calculated the polarized reflectivity spectra originating from interband transitions. In Fig. 8 the specular reflectivity, calculated from ϵ^{xx} (thick solid line), ϵ^{yy} (thick dashed line), and ϵ^{zz} (thick dot-dashed line) is compared with the experimental reflectivity spectra. The experimental spectrum with the electric field polarized parallel to the b axis (thin dashed line) should be directly compared with our spectrum calculated from ϵ^{yy}. The other experimental spectrum (thin solid line) closely but not completely, corresponds to our spectrum calculated using ϵ^{xx}. Clearly, the agreement is not too good. All three theoretical spectra have a distinct minimum around 7 eV with only a small variation, whereas this minima in the experimental spectra seems to occur at 6 eV for $E\|b$ while for $E\perp b$ no clear minimum is observed. We also see that whereas the amplitudes of the peaks at 2.6 eV is very different in the experimental spectra, the corresponding peaks in the calculated spectra have about the same amplitude. There is, however, some relative agreement if one compares the differences between the two experimental spectra and the differences between the corresponding calculated spectra. The amplitude of the experimental and theoretical $E\|b$ spectra is significantly lower than the amplitude of the theoretical $E\|x$ and $E\perp b$ spectra, respectively. There is also some correspondence in the positions of the peaks and valley at lower energies. In general, if indirect transitions are taken into account a certain broadening of the maxima takes place.[29] Up to 7 eV, the reflectivity with polarization parallel to c is higher than for the other two directions. This is due to the presence of narrow bands in the conduction band along the Γ-Z direction of the Brillouin zone, see Fig. 4. It should be noted that the absolute value of the theoretical reflectivity is much larger than the experimental. The possible reasons for the discrepancy between theory and experiment may be due to the following. The reflectivity spectra for SnI_2 was measured using synchrotron radiation with small samples and hence, it is difficult to obtain the absolute value of the reflectivity.[9] Fujita *et al.*[7] therefore assumed that the reflectivity in the transparent region is the same as that calculated from the room temperature refractive indices given by Kostyshin *et al.*[4] In general, the reflectivity near the absorption edge increases as the temperature decreases.

The reflectivity spectra can be split into two regions; the first is below 7 eV and is due to cationic excitations and the other, above 7 eV, is mainly arising from anionic excitations. Up to about 4.5 eV, the reflectivity spectra arise mainly from the Sn(2a) $5s \rightarrow$ Sn(4i) $5p$ interband transitions. Between 4.5 and 7 eV, the main contributions come from Sn(4i) $5s \rightarrow$ Sn(2a) $5p$ interband transitions and Sn(2a) $5s \rightarrow$ Sn(4i) $5p$ transitions. The valleys in the reflectivity spectra around 7 eV indicate the onset of cationic excitations and above this energy anionic excitations dominate, i.e., interband transitions from I $5p \rightarrow$ I $5d$. This is evident from the site and angular momentum decomposed DOS (Fig. 2) and band structure (Fig. 6).

In our calculated reflectivity spectra for $E\|b$, the reflectance was 0.38 at $\hbar\omega = 2.3$ eV, whereas the experimentally measured value at this energy is 0.26 only. We have made several attempts to improve the agreement between theory and experiment in the reflectivity spectra of SnI_2. This includes additional basis sets, the increase in the number of k points in the BZ sum, etc. We obtained virtually the same

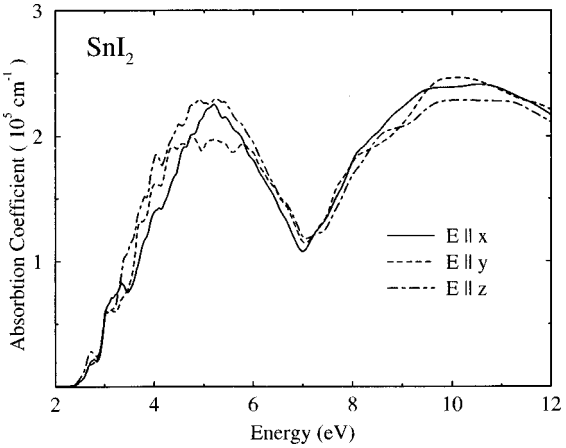

FIG. 9. Calculated absorption coefficient spectra of SnI_2 for the three polarization directions. The spectra are slightly broadened, see text.

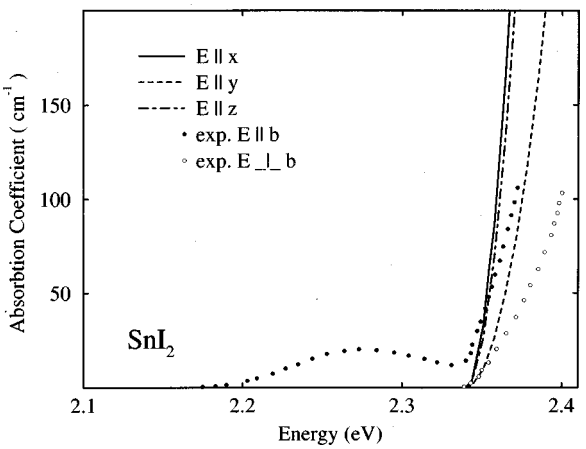

FIG. 10. Calculated and experimental absorption coefficient spectra of SnI_2 at the absorption edge. The calculated spectra are not broadened. Experimental data were measured by Ohno, Yoshida, and Fujita (Ref. 8).

result for the optical properties and we conclude that the remaining discrepancies, such as the absolute position and the width of the peaks, cannot be attributed to the computational procedures for the electronic structure calculation. We suggest that more experimental studies on high-energy polarized reflectivity measurements are needed to confirm our results.

Very recently Ohno *et al.*[8] measured the polarized optical absorption edge for SnI_2 as a function of temperature. In the polarized direction $E\|b$ they have found a peak just below the sharp absorption edge. In order to understand the origin of this low-energy absorption peak in $E\|b$, we have also calculated the polarized absorption spectra shown in Fig. 9. From the absorption spectra in Fig. 9, it is immediately obvious why the color of SnI_2 should be reddish because the absorption starts around 2.35 eV. This is the high-frequency region of the visible spectrum, i.e., green light. Thus, low frequencies are not absorbed and they will therefore dominate the transmitted light. As a consequence, the crystal will appear red, just as a thin gold film appears green due to the high absorption in the low-frequency part of the spectrum. The absorption coefficients, shown in Fig. 9, have peaks around 5 eV and 10 eV and a minimum around 7 eV, for all polarization directions. The anisotropy causes the $E\|y$ absorption to be somewhat lower than for the other two polarization directions at 5 eV. All three spectra rise steeply at the absorption edge, for a blowup see Fig. 10. In Fig. 10 we have also plotted the experimental absorption edge spectra, measured at 10 K.[8] It is interesting to note that the experimentally observed broad absorption peak feature between 2.2 and 2.3 eV at $E\|b$ is not present in the theoretical spectra. We conclude that the origin of this peak is not due to direct interband transitions. Ohno *et al.*[8] interpreted that the origin of this peak is an excitonic effect. The interband optical calculation does not include this excitonic effect. This may be a possible reason for the absence of the experimentally observed lowest-energy absorption peak in our theoretical curve, although excitons normally produce sharper features. Our band-structure calculations show that the fundamental gap is of indirect type and hence the lowest-energy excitation could also be due to indirect interband transition. As we have only considered direct interband transitions in our calculations, such a peak cannot appear in the theoretical spectra. It has been suggested by Doni *et al.*[10] that it is due to phonon assisted transitions over the indirect gap. This suggestion compares well with our calculated indirect band gap.

In order to clarify the discrepancy between experiment and theory regarding optical absorption spectra near the fundamental edge (Fig. 10) Yoshida *et al.*[30] recently made experimental studies using highly purified SnI_2 single crystals obtained from the zone-refining method at 6 K. Interestingly, they have found that the broad absorption peak around 2.275 eV in the previous experimental studies are not present and also the polarized absorption spectra obtained near the fundamental edge are found to be in good agreement with the theoretical results given in Fig. 10. Further, they have repeated their absorption studies near the fundamental edge using the less purified crystals obtained from the Bridgeman method at 8 K. In this case they are able to reproduce the broad absorption peak around 2.275 eV like the previous experimental studies. Hence, the discrepancy between the experimental and theoretical optical spectra is due to the small amount of impurities present at SnI_2 in the previous experimental studies. Unfortunately no experimental reflectivity spectra for highly purified SnI_2 crystals at low temperatures are available to compare our results. We hope the present results will motivate more experimental studies in the future.

The dispersive parts of the diagonal elements of the dielectric tensor are shown in Fig. 11. The dichroism is clearly visible, especially in the low-energy parts of the spectra. The function representing characteristic energy losses (or plasmon oscillations) is one of the more important among those suitable for the description of microscopic and macroscopic properties of solids. This function is proportional to the probability that a fast electron moving across a medium loses an energy E per unit length. The electron energy-loss spectra (EELS) for SnI_2 calculated from the dielectric functions for the three different polarization directions are shown in Fig. 12. Generally speaking, the most prominent peak in the EELS spectrum is identified as the plasmon peak, signaling the energy of collective excitations of the electronic charge density in the crystal. It is possible to have several plasmon peaks in a crystal. In this context we should also mention the occurrence of plasma resonances and their coupling to the

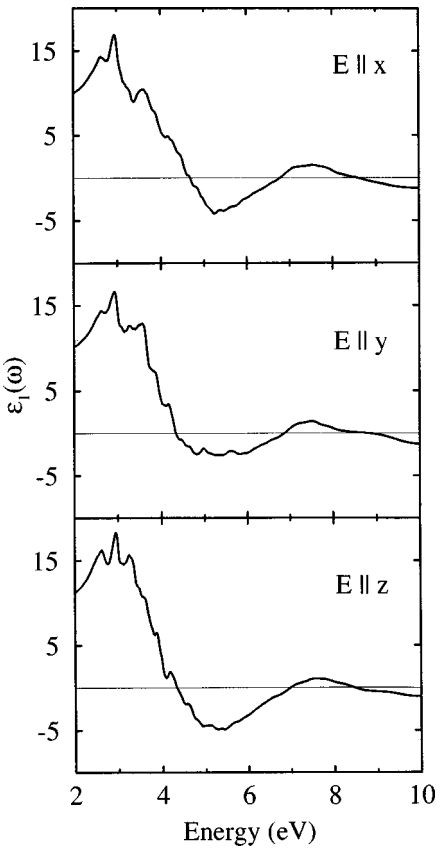

FIG. 11. The real parts of the diagonal elements of the dielectric tensor of SnI_2 with spin-orbit coupling. The spectra are slightly broadened, see text.

spectra in Fig. 11. Plasma resonances manifest themselves as rather distinct peaks in the electron energy-loss spectra, and are thus a feature that should be relatively easy to observe experimentally. However, they also have a simple relationship to the dispersive part of the dielectric function. A root in ϵ_1, i.e., $\epsilon_1=0$, can give rise to a plasma resonance, although this is not a sufficient requirement. Damping of the plasma oscillations, so-called Landau damping, may suppress the plasma peaks in the experiments.[31] Nevertheless, it is interesting to note the positions of these roots. In the region

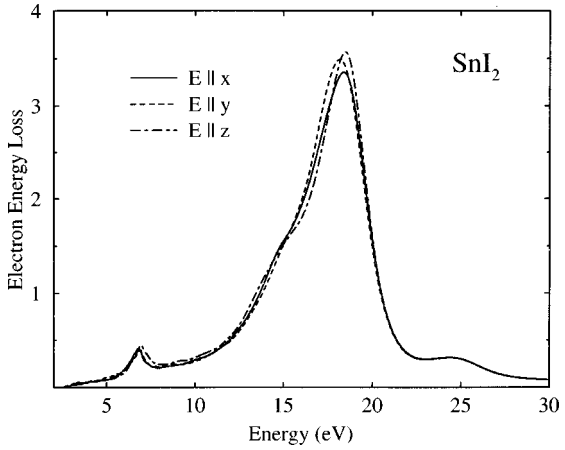

FIG. 12. The electron energy-loss function of SnI_2 calculated from the diagonal elements of the dielectric tensor. The spectra are slightly broadened, see text.

$2-10$ eV we can identify three roots in the spectra. The first root is situated at 4.6 eV for the $E\|x$ spectrum and somewhat lower, 4.3 eV, for the other two spectra. The next root is found around 6.9 eV for the $E\|x$ spectrum and at 6.8 eV for the other two. The third root is situated around 8.5 eV in all three spectra. There is also a fourth root at 19 eV (not shown). At such high energies the ϵ_1 spectra are very flat and the amplitude of the ϵ_2 spectra is small.

There are four prominent features in the EELS spectra: two distinct peaks at 7 eV and 19 eV and two broader features around 15 eV and 25 eV. The anisotropy is especially visible in the highest of the peaks, i.e., the one at 19 eV. The two peaks both correspond to roots in the ϵ_1 spectra. However, as is now obvious, not all roots to $\epsilon_1=0$ give rise to peaks in the electron energy-loss spectrum. Thus $\epsilon_1=0$ is a necessary condition for plasma oscillations to occur, but as observed is not a sufficient condition.

In order to compare our theoretical value of the dielectric constant at zero frequency with experimental values we have estimated the average value of zero frequency dielectric constant using the relation $\epsilon(0)=1/3[\epsilon^{xx}(0)+\epsilon^{yy}(0)+\epsilon^{zz}(0)]$, where $\epsilon^{xx}(0)$, $\epsilon^{yy}(0)$, and $\epsilon^{zz}(0)$ are the zero frequency dielectric constant along the crystal axes. From this relation, the estimated average zero frequency dielectric constant is 8.87. These values are found to be comparable with the value 11.30 measured using microwave frequencies of 8.95 GHz on powder sample.[6] The polarized zero frequency dielectric constants obtained parallel to the a, b, and c axes of the crystal are 8.83, 9.79, and 9.01, respectively. These results clearly indicate the anisotropy in the optical properties of SnI_2. Unfortunately no experimental polarized zero frequency dielectric constant is available to compare our results with.

VI. CONCLUSIONS

A detailed analysis of the electronic structure of SnI_2 has been performed using the FP-LMTO method as well as the TB-LMTO method. The chemical bonding between tin and iodine in SnI_2 was demonstrated to be of mostly ionic nature with an additional covalent contribution, which was established through analysis of the charge-density distribution as well as the site and angular momentum decomposed density of states. The overall topology of the polarized reflectivity spectra obtained from our first principle calculations is unfortunately found to be in considerably worse agreement with experiment than expected. Previous calculations of optical properties for other systems, using the very same method, have been found to be in extremely good agreement with experimental results not only for isotropic systems such as IVB refractory metal compounds[20] but also for highly anisotropic systems such as graphite.[19] Therefore it is very surprising that the agreement in the present case is relatively poor. We also glanced at the absorption edge spectrum measured by Ohno, Yoshida, and Fujita when determining how much the gap needs to be shifted. Unfortunately, the position of the edge seems to be very temperature dependent, making an estimation of the 0 K edge position so uncertain that this method did not improve our precision.

The nature of the fundamental gap in this material was found to be indirect, irrespective of the band-structure

method used in the calculations. The indirect band gap is followed by a direct gap appearing at the Z point of the Brillouin zone. Our band-structure results are in good agreement with conclusions drawn from optical measurements by Gorban *et al.*[2] and consistent with the band-structure studies made by Doni *et al.*[10] from the semiempirical tight-binding method. As our band structures show, the top of the valence band contains Sn(2a) $5s$ character and the bottom-most valence band is from Sn(4i) $5p$ states, implying that the experimentally observed peak at 2.56 eV is due to Sn(2a) $5s \rightarrow$Sn(4i) $5p$ transitions. The absorption peak at 2.275 eV for $E\|b$ polarization is not present in our absorption spectra and hence we conclude that the origin of this peak is not due to direct interband transitions. Furthermore, new experiments reveal that this structure disappears when the crystal is grown using the zone-melting method instead of the Bridgman-Stockbarger technique.[30] More low-temperature single crystal polarized optical property studies are needed to confirm the nature of the band gap. Finally, the electronic structure of SnI_2 as calculated by the atomic sphere approximation has been shown to be very similar to the electronic structure of a more accurate method where no approximations concerning the shape of the electron density or potential are made.

ACKNOWLEDGMENTS

We are thankful for financial support from the Swedish Natural Science Research Council and for support from the materials science consortium No. 9. We are also grateful to O. K. Andersen, O. Jepsen, and A. Burkhardt for providing their latest version of the TB-LMTO program for the present band-structure analysis. We are also grateful to H. Yoshida, N. Ohno, and M. Fujita for communicating their results prior to publication. L. Nordström and L. Fast are acknowledged for useful discussions. A.D. wishes to acknowledge C. G. Ribbing for many enlightening discussions.

[1] J. M. Ricart, J. Rubio, and F. Illas, Chem. Phys. Lett. **123**, 528 (1986); S. Stranges, M. Y. Adam, C. Cauletti, M. de Simone, C. Furlani, M. N. Piancastelli, P. Decleva, and A. Lisini, J. Chem. Phys. **97**, 4764 (1992).

[2] I. S. Gorban, V. F. Gorchen, and T. N. Sushevich, Fiz. Tverd. Tela (Leningrad) **18**, 2095 (1976) [Sov. Phys. Solid State **18**, 1220 (1976)].

[3] R. J. Zollweg and L. S. Forst, Bull. Am. Phys. Soc. **11**, 745 (1966).

[4] M. T. Kostyshin, V. S. Kostko, I. Z. Indutnyi, and V. M. Kosarev, Opt. Spektrosk. **52**, 182 (1982) [Opt. Spectrosc. **52**, 108 (1982)].

[5] M. Benavides-Garcia and K. Balasubramanian, J. Chem. Phys. **100**, 2821 (1994).

[6] C. C. Desai, J. L. Rai, and A. D. Vyas, J. Mater. Sci. **17**, 3249 (1982).

[7] M. Fujita, K. Hayakawa, K. Fukui, M. Kitaura, H. Nakagawa, and T. Miyanaga, J. Phys. Soc. Jpn. **65**, 605 (1996).

[8] N. Ohno, H. Yoshida, and M. Fujita, in *Proceeding of the 2nd International Conference on Excitonic Processes in Condensed Matter (EXCON'96)*, edited by. S. Michael (Kurort, Gohrisch, Germany, 1996), p. 71.

[9] M. Fujita (private communications).

[10] E. Doni, G. Grosso, and I. Ladiana, Physica B & C **99B**, 281 (1980).

[11] O. K. Andersen, Phys. Rev. B **12**, 3060 (1975); O. K. Andersen and O. Jepsen, Phys. Rev. Lett. **53**, 2571 (1984); O. K.Andersen, O. Jepsen, and D. Glötzel, in *Highlights of Condensed-Matter Theory*, edited by F. Bassani, F. Fumi, and M. P. Tosi (North-Holland, New York, 1985); W. R. L. Lambrecht and O. K. Andersen, Phys. Rev. B **34**, 2439 (1986); P. Blöchl, O. Jepsen, and O. K. Andersen, *ibid.* **49**, 16 223 (1994).

[12] O. Jepsen and O. K. Andersen, Z. Phys. B **97**, 35 (1995).

[13] J. M. Wills (unpublished); J. M. Wills and B. R. Cooper, Phys. Rev. B **36**, 3809 (1987); D. L. Price and B. R. Cooper, *ibid.* **39**, 4945 (1989).

[14] D. J. Chadi and M. L. Cohen, Phys. Rev. B **8**, 5747 (1973); S. Froyen, *ibid.* **39**, 3168 (1989).

[15] U. von Barth and L. Hedin, J. Phys. C **5**, 1629 (1972); J. F. Janak, V. L. Moruzzi, and A. R. Williams, Phys. Rev. B **12**, 1257 (1975).

[16] J. Callaway, *Quantum Theory of the Solid State* (Academic Press, New York, 1974), Pt. B.

[17] H. Ehrenreich and M. H. Cohen, Phys. Rev. **115**, 786 (1959).

[18] N. V. Smith, Phys. Rev. B **3**, 1862 (1971).

[19] M. Alouani and J. M. Wills, Phys. Rev. B **54**, 2480 (1996); R. Ahuja, S. Auluck, J. M. Wills, M. Alouani, B. Johansson, and O. Eriksson, *ibid.* **55**, 4999 (1996).

[20] A. Delin, O. Eriksson, R. Ahuja, B. Johansson, M. S. S. Brooks, T. Gasche, S. Auluck, and J. M. Wills, Phys. Rev. B **54**, 1673 (1996).

[21] R. A. Howie, W. Moser, and I. C. Trevena, Acta Crystallogr. Sect B **28**, 2965 (1972).

[22] T. J. Bastow and H. J. Whitfield, J. Magn. Reson. **37**, 269 (1980).

[23] L. Pauling, *The Nature of Chemical Bond* (Cornell University Press, Ithaca, New York, 1960).

[24] V. L. Maruzzi, P. Oelhafen, and A. R. Williams, Phys. Rev. B **27**, 7194 (1983); P. Ravindran and R. Asokamani, *ibid.* **50**, 668 (1994).

[25] C. S. Wang and W. E. Pickett, Phys. Rev. Lett. **51**, 597 (1983).

[26] R. M. Dreizler and E. K. U. Gross, *Density Functional Theory, An Approach to the Quantum Many-Body Problem* (Springer-Verlag, Berlin, 1990).

[27] F. Bechstedt and R. Del Sole, Phys. Rev. B **38**, 7710 (1988).

[28] R. W. Godby, M. Schlüter, and L. J. Sham, Phys. Rev. Lett. **56**, 2415 (1986).

[29] V. E. Egorushkin, A. I. Kulmentiev, E. V. Savushkin, A. B. Kononenko, and S. V. Alyshev, *Electrons and Phonons in Disordered Alloys* (Nauka-sib, Otdelenie, Novosibirsk, 1989), p. 272.

[30] H. Yoshida, N. Ohno, and M. Fujita, Phys. Status Solidi B (to be published).

[31] See, for instance, C. Kittel, *Quantum Theory of Solids* (Wiley, New York, 1987), p. 301.